

## Replica theory and large-D Josephson junction hypercubic models

This article has been downloaded from IOPscience. Please scroll down to see the full text article.

1995 J. Phys. A: Math. Gen. 28 4481

(<http://iopscience.iop.org/0305-4470/28/16/008>)

View [the table of contents for this issue](#), or go to the [journal homepage](#) for more

Download details:

IP Address: 171.66.16.68

The article was downloaded on 02/06/2010 at 00:47

Please note that [terms and conditions apply](#).

# Replica theory and large- $D$ Josephson junction hypercubic models

Enzo Marinari<sup>†||</sup>, Giorgio Parisi<sup>‡¶</sup> and Felix Ritort<sup>§+</sup>

<sup>†</sup> Dipartimento di Fisica and INFN, Università di Cagliari, Via Ospedale 72, 09100 Cagliari, Italy

<sup>‡</sup> Dipartimento di Fisica and INFN, Università di Roma 'La Sapienza' Piazzale Aldo Moro 2, 00185 Rome, Italy

<sup>§</sup> Departamento de Matematica Aplicada, Universidad Carlos III de Madrid, Calle Butarque 15, 28911 Leganes, Madrid, Spain

Received 20 February 1995

**Abstract.** We study the statistical mechanics of a  $D$ -dimensional array of Josephson junctions in the presence of a magnetic field on a lattice of side 2. In the high-temperature region the thermodynamical properties can be computed in the limit  $D \rightarrow \infty$ . A conjectural form of the thermodynamic properties in the low-temperature phase is obtained by assuming that they are the same as an appropriate spin-glass system, based on quenched disordered couplings. Numerical simulations show that this conjecture is very accurate in one regime of the magnetic field, while it is probably slightly inaccurate in a second regime.

## 1. Introduction

In this paper we pursue our research programme on the relation between systems based on a Hamiltonian containing quenched disorder and systems with a fixed frustrated but non-random Hamiltonian [1, 2]. Here we study the statistical mechanics of arrays of Josephson junctions [3] in  $D$  dimensions, in the limit where  $D \rightarrow \infty$  on a lattice of size 2 (i.e. on a single hypercube with  $2^D$  points). The case of a fully-frustrated lattice has been already discussed in [4].

In the framework of the spherical approximation the thermodynamic properties can be computed by using the results obtained in [3]. It is possible to prove that the spherical approximation gives the correct results even for the  $XY$  model (the one that will mainly interest us here) in the high-temperature phase. At  $T = T_c$  the system undergoes a phase transition. In the low-temperature region the spherical approximation breaks down. We conjecture that the thermodynamical properties of the system are the same as an appropriate spin-glass model, constructed in such a way as to have the same high-temperature expansion as the original deterministic model. We solve the disordered model by using the replica approach.

We have simulated numerically systems of dimension  $D$ , ranging from 3 to 16. We find that the comparison of the numerical simulation with the theoretical results is extremely good in the high-temperature phase (as expected). In the low-temperature phase things

<sup>||</sup> E-mail address: marinari@ca.infn.it

<sup>¶</sup> E-mail address: parisi@roma1.infn.it

<sup>+</sup> E-mail address: ritort@dulcinea.uc3m.es

seem to work quite well when we move toward the fully-frustrated model (starting from a magnetic field  $\theta = \frac{\pi}{2}$  and increasing  $\theta$ ), but when decreasing  $\theta$  (towards the ferromagnetic system) we find a rather disturbing phenomenon. Indeed, in this region a naive extrapolation for  $D \rightarrow \infty$  gives a result which differs slightly from the analytic results (obtained by applying replica theory to the model which contains quenched disorder). Such a discrepancy becomes larger and larger when decreasing the frustration. We are unable to decide if in this regime our analytic results are only a good approximation to the behaviour of the system without quenched disorder, or if they are exact and the finite- $D$  corrections have a peculiar dependence on  $D$ . An analytic computation inside our theoretical framework of the  $\frac{1}{D}$  corrections would be extremely useful, but goes beyond the aims of this paper.

In section 2 we give a short summary of the results obtained in [3]. In section 3 we describe our strategy, and define the model with quenched disorder which we will *substitute* for the original deterministic model. In section 4 we will discuss the high- $T$  expansion. In section 5 we will use replica theory to solve the random model for  $T < T_c$ . In section 6 we will describe our numerical simulations, and compare them to the analytic results obtained in the former sections. Finally, in the appendix we close a gap in the proof of [3] about the connection of the high-temperature expansion and the Green functions of the  $q$ -deformed harmonic oscillator.

## 2. Diagram counting, Josephson junctions and $q$ -deformations

We will start here by defining the relevant statistical models, and by reviewing in a very cursory manner the results of [3]. The prototype model is the Gaussian model, defined by the Hamiltonian

$$\beta H_G \equiv -\beta \Re \left\{ c(D) \sum_{j,k} \eta_j^* U_{j,k} \eta_k \right\} + \frac{1}{2} \sum_k |\eta_k|^2. \quad (1)$$

Here  $c(D)$  is a normalization constant, which will be useful later to rescale the Hamiltonian in order to obtain a non-trivial limit when  $D$  goes to infinity.  $c(D)$  will be  $\frac{1}{2D}$  for the usual ferromagnetic  $XY$  model (and in this case we will get a phase transition at  $\beta = 1$ ). For a model with random couplings, and for the frustrated models we will be mainly discussing in this paper, we will have to take  $c(D) \simeq (2D)^{-1/2}$  in order to ensure a sensible infinite-dimensional limit.

The real and imaginary parts of the complex  $\eta_j$  lattice variables can take values that range from  $-\infty$  to  $+\infty$ . We will consistently indicate with  $\eta$  the fields of the Gaussian model. With  $\phi_i$  we will denote the fields of the  $XY$  model, which are constrained to be, on every site, of modulus 1, i.e. for all sites  $i$

$$|\phi_i|^2 = 1. \quad (2)$$

Their dynamics are governed by the Hamiltonian

$$\beta H_{XY} \equiv -\beta \Re \left\{ c(D) \sum_{j,k} \phi_j^* U_{j,k} \phi_k \right\}. \quad (3)$$

With  $\sigma_i$  we will denote the fields of the spherical model, which satisfy the constraint

$$\sum_i |\sigma_i|^2 = N \quad (4)$$

with the Hamiltonian

$$\beta H_S \equiv -\beta \Re \left\{ c(D) \sum_{j,k} \sigma_j^* U_{j,k} \sigma_k \right\}. \quad (5)$$

We can rewrite the spherical model Hamiltonian by including the constraint by means of a Lagrange multiplier  $\mu$ . We can write

$$\beta H_S \equiv -\beta \Re \left\{ c(D) \sum_{j,k} \sigma_j^* U_{j,k} \sigma_k \right\} + \mu \left( \sum_i |\sigma_i|^2 - N \right) \quad (6)$$

for unconstrained variables. Integration over  $\mu$  ensures that the spherical constraint is implemented.

The  $U$  couplings are non-zero only for the first neighbouring site couples. They are complex numbers of modulus 1. In the following we will always have that

$$U_{j,i} = U_{i,j}^* \quad (7)$$

i.e. the link couplings are oriented, and when coming back on a link one takes the opposite phase to when following it in the positive direction. Using the language of gauge theories one says that the  $U$  couplings are  $U(1)$  lattice gauge fields [5].

Here we will be discussing hypercubic models. For a  $D$ -dimensional model the field variables live on a  $D$ -dimensional hypercube which is made of  $2^D$  points. We only include link couplings which are internal to the cube, i.e. we use open boundary conditions. The number of independent link couplings in our lattice is  $D2^{D-1}$ . In this approach the limit of a large number of dimensions is taken by letting the dimensionality of the hypercube increase (as opposed to the usual limit of an infinite-range interaction).

Apart from the two cases we have already quoted (i.e. the ferromagnetic model with all  $U$  fields equal to 1 and the  $XY$  spin glass, where  $U_{j,k} = \exp(ir_{j,k})$ , and the  $r_{j,k}$  are random numbers uniformly distributed in the interval  $(0, 2\pi]$ ) we will mainly be interested here in models where the couplings are such as to generate a constant magnetic field  $\theta$ . The magnetic field which flows to a given elementary plaquette  $\mathcal{P}$  is†

$$\prod_{\mathcal{P}} U_{\mathcal{P}} = e^{\pm i\theta_{\mathcal{P}}} \quad (8)$$

where the sign of the exponents determines if the field is flowing in the positive or in the negative direction. We will be interested in the case where  $\theta_{\mathcal{P}} = \theta$  is constant on all the lattice, i.e. the plaquettes undergo a constant, uniform frustration. The case  $\theta = 0$  gives the ferromagnetic model, while the case  $\theta = \pi$  gives the fully-frustrated model, which we have discussed in detail in [4]. If we let  $\theta_{\mathcal{P}}$  be a random variable we obtain a so-called *gauge glass* [6–8].

The values of the signs of the exponents that enter (8) are in part arbitrary. Parallel plaquettes have to be cut by a flux flowing in the same direction, i.e. the signs must have the structure  $\mathcal{S}_{\alpha,\beta}$ , where  $\mathcal{S}$  is a tensor, which is automatically antisymmetric because of the way we have defined the  $U$  fields. We are interested in the choice of a *generic* structure of  $\mathcal{S}$  (for the reasons we have discussed in [1, 2] and we will discuss more fully in the following). We need a generic representative of the ensemble of the possible choices of  $\mathcal{S}$ . One can see that for  $D > 3$  the choice  $\mathcal{S}_{\alpha,\beta} = 1$  is not a good choice (this is not true in 3 and  $2D$ , where all choices of  $\mathcal{S}$  are equivalent). We also need to define the parameter

$$q \equiv \cos(\theta) \quad (9)$$

which will play an important role in the following.

Let us be more explicit and summarize. Our model lives in a magnetic field given by the antisymmetric tensor

$$\theta_{\alpha,\beta} = \mathcal{S}_{\alpha,\beta} \theta \quad (10)$$

† The plaquette is the elementary lattice closed circuit, made from four oriented links forming a minimal square.

where in the continuum  $\theta_{\alpha,\beta}$  becomes  $\partial_\alpha A_\beta - \partial_\beta A_\alpha$ . This is a condition of complex frustration on the elementary plaquettes. For  $\theta = \pi$  we recover the fully-frustrated model. On our hypercubic lattice the construction of the  $U$  fields that generate a  $\theta$  frustration is unique modulo gauge transformations, and can be easily given. We define  $U_\mu(j)$  as the coupling  $U$  which goes from site  $j$  in direction  $\mu$  (we only have first neighbour non-zero coupling).  $\mu$  goes from 1 to  $D$ , since we only need to set couplings in the positive direction (the one going in the negative direction is set by the relation (7)). We set

$$U_1(j) = 1 \tag{11}$$

and for  $\mu > 1$

$$U_\mu(j) = e^{i\theta \sum_{\nu=1}^{\mu-1} S_{\mu,\nu} j_\nu} \tag{12}$$

For example, in four dimensions we get

$$\begin{aligned} U_1(j) &= 1 & U_2(j) &= e^{i\theta(S_{2,1}j_1)} \\ U_3(j) &= e^{i\theta(S_{3,1}j_1+S_{3,2}j_2)} & U_4(j) &= e^{i\theta(S_{4,1}j_1+S_{3,2}j_2+S_{3,3}j_3)} \end{aligned}$$

In this paper we will obtain a generic  $\mathcal{S}$  by picking up at random the  $\pm 1$  components of the antisymmetric tensor  $S_{\alpha,\beta}$ . This is only a small amount of randomness. The system is determined by  $D2^{D-1}$  couplings, i.e. a number of couplings exponentially large in  $D$ , while we are using only order of  $D^2$  random numbers to pick up phases which make the magnetic field tensor generic. It is maybe possible to imagine simple forms of the tensor  $\mathcal{S}$  which give a generic magnetic field (i.e. with the correct moments).

Let us start from the discussion of the Gaussian model, where the  $\eta$  fields are unconstrained (equation (1)), and summarize the steps taken in [3]. Later we will introduce the modifications needed to discuss the XY (equations (2), (3)) and the spherical model (equations (4), (5)). We will assume in the following that we are taking the  $D \rightarrow \infty$  limit by the hypercubic lattice approach we have described previously.

On general grounds the free energy  $F$  of a statistical model like the ones we have defined in (1), (3) and (5) can be written through its *high-temperature expansion* as [9]

$$\beta F(\beta) = \sum_n \frac{(\beta c(D))^n}{n} \mathcal{N}(n) \langle W(C) \rangle_n \tag{13}$$

where the sum runs over all oriented circuit lengths  $n$ ,  $\mathcal{N}(n)$  is the number of rooted closed circuits of length  $n$ , and  $\langle W(C) \rangle_n$  is the average over all circuits of length  $n$  of the value of the Wilson loop  $W(C)$  (defined as the oriented product of the couplings that one encounters when following the closed circuit). We will be interested in the  $D \rightarrow \infty$  limit, and define

$$G_n^{(q)} = \lim_{D \rightarrow \infty} (2D)^{-n/2} \mathcal{N}(n) \langle W(C) \rangle_n \tag{14}$$

With the superscript  $(q)$  we are indicating the dependence of  $G$  over the value of  $\theta$ , i.e. of  $q$ . Using this definition in the  $D \rightarrow \infty$  limit the free energy reads

$$\beta F(\beta) = \sum_n \frac{\beta^n G_n^{(q)}}{n} \tag{15}$$

In order to obtain the free energy of the system we will have to compute the functions  $G_n^{(q)}$ .

In the ferromagnetic case (where  $\theta = 0$  and  $q = 1$ ) everything is easy, since  $\langle W(C) \rangle_n = 1$  for all values of  $n$ . Here it is easy to recover all the usual results of the high- $T$  expansion in the  $D \rightarrow \infty$  limit [3].

The next step can be started by discussing the  $D \rightarrow \infty$  limit of a Gaussian, XY or spherical spin glass, i.e. the situation where  $U_{j,k} = \exp(ir_{j,k})$ , and the  $r_{j,k}$  are random

numbers uniformly distributed in the interval  $(0, 2\pi]$ , and one eventually averages over the  $r$  random variables. We have already reminded the reader that this is a usual spin glass (the replica-symmetric solution for the  $XY$  case is already discussed in [10]). This is not one of the non-random models that we want to study here, but we are using it just in order to go back to our models in the magnetic field  $\theta$  with a bit more knowledge. In this case one can easily see that the only (closed) diagrams contributing to the free energy are *backtracking* diagrams. For any steps going from  $i$  to  $j$  we need the opposite step going from  $j$  to  $i$ , or the integrals over the quenched  $r$  variables give us zero.

This step is completed by noticing that the backtracking diagrams are also the only ones which survive (in the  $D \rightarrow \infty$  limit) in the  $\theta = \frac{\pi}{2}$  model, which we call *half frustrated*. Here on all elementary plaquettes the product of the plaquette couplings is purely imaginary,  $\pm i$ . It is easy to see why. In the  $D \rightarrow \infty$  limit each step is taken in a different direction. So each time we find a phase  $i$  which enters our Wilson loop, we will have to consider the contribution of another path with the conjugate phase  $-i$  (in  $D$  finite two steps in the same direction can create a situation where this cancellation no longer holds).

In this way we have associated backtracking diagrams to one particular case of our frustrated models, the one in which  $\theta = \frac{\pi}{2}$ , and the plaquette frustration has the constant imaginary value  $i$  (apart from a sign). The next step consists of associating to each backtracking diagram a planar diagram.

The instructions are the following. In order to compute  $G_{2n}^{(0)}$  consider  $2n$  letters, equal at couples, i.e. take two  $a$ 's, two  $b$ 's, two  $c$ 's, up to  $n$  couples. The letters represent the different directions of the path. To form a closed path one has to come back in all selected directions. Form a word by ordering these letters, and put the ordered letters on a circle. Now connect equal letters with lines. Count the number of intersections of these lines. Call  $I_n(m)$  the number of words done of  $n$  couples which have  $m$  intersections.  $I_n(m)$  is a topological invariant, and only depends on the order of the letters. The condition of zero intersections implies that the diagram is planar. One has that, for the Gaussian model,

$$G_n^{(0)} = I_n(0). \quad (16)$$

This shows [3] that the problem of the Gaussian half-frustrated model (and of the Gaussian spin glass) is solved by counting planar diagrams.  $I_n(0)$  has been computed in [11], and the generalization to the  $XY$  and spherical model is straightforward.

The next step of the deduction of [3] is the one that concerns our model which lives in a constant magnetic field. It is a generalization of the counting argument discussed before, and it says that we can solve our problem by counting non-planar diagrams, i.e. by counting words which have a non-zero number of intersections. There are two crucial results. The first states that, in a large number of dimensions  $D$ ,

$$G_{2n}^{(q)} = \sum_{w(2n)} q^{A(w(2n))} \quad (17)$$

where  $A(w)$  is the signed area associated with the diagram represented by the word  $w$ . Planar diagrams, with zero intersections, have zero area. In the  $D \rightarrow \infty$  limit all the steps which form the diagram are taken in different directions, and the projected signed area over the plane  $(\mu, \nu)$   $A_{\mu,\nu}$  can only take the values 0 and  $\pm 1$ . The total area  $A$  has been defined as the sum of the modulus of the individual signed areas

$$A \equiv \sum |A_{\mu,\nu}|. \quad (18)$$

The second part of this step shows that  $A(w)$  is equal to the number of intersections of the line drawing associated to the word  $w$ . Considering diagrams which have a non-zero area means considering words whose line drawings have a non-zero number of intersections.

This generalization of the counting of planar diagrams to a counting on non-planar diagrams has shown in a last step to have an underlying powerful algebraic structure. Indeed [3] shows that (and we complete the proof of this statement here)

$$G_{2n}^{(q)} = \sum_{w(2n)} q^{A(w(2n))} = \langle 0 | \mathcal{X}_q^{2n} | 0 \rangle \quad (19)$$

where the operator  $\mathcal{X}_q$  is

$$\mathcal{X}_q = \mathcal{R}_q + \mathcal{L}_q \quad (20)$$

and the operators  $\mathcal{L}_q$  and  $\mathcal{R}_q$  satisfy the commutation relations of the annihilation and the creation operators of a  $q$ -deformed harmonic oscillator

$$\mathcal{L}_q \mathcal{R}_q - q \mathcal{R}_q \mathcal{L}_q = 1. \quad (21)$$

The vacuum state  $|0\rangle$  (for the model with charge  $q$ ) is defined by the condition

$$\mathcal{L}_q |0\rangle = 0. \quad (22)$$

$\mathcal{L}_q$  may be identified with the annihilation operator and  $\mathcal{R}_q$  with the creation operator for a  $q$ -deformed harmonic oscillator. They can be represented as

$$\begin{aligned} \mathcal{R}_q |m\rangle &= [m]_q^{1/2} |m+1\rangle \\ \mathcal{L}_q |m\rangle &= [m-1]_q^{1/2} |m-1\rangle \end{aligned} \quad (23)$$

where

$$[m]_q \equiv \frac{1 - q^{m+1}}{1 - q} \quad (24)$$

and  $m$  takes integral values in the interval  $(0 - \infty]$ .

For  $q = 1$  we have the usual ferromagnet, for  $q = -1$  the fully-frustrated model [4], and for  $q = 0$  our half-frustrated model (which has the same diagrammatic expansion as the spin-glass model).

These are the basis on which we will try to build here, mainly trying to gather information about the behaviour of these frustrated models in the low- $T$ , glassy phase.

### 3. Our strategy and the definition of the random model

Here we will use a strategy we have introduced in [1, 2] (see also [12] for the development of closely connected ideas). We start with a model which does not contain quenched disorder, but that is complex enough to make us suspicious of the possible presence of a spin-glass-like phase for temperatures  $T$  low enough. We look for a model which contains quenched disorder, and that is similar enough to the original model to have potentially the same behaviour (even in the low- $T$  phase, if we are very ambitious). Replica theory allows us to solve the random model, and to try and get information about the deterministic model. References [1, 2] discuss successful examples of the use of this strategy.

Here we will adopt the same approach. We will introduce a model containing random quenched disorder. In this new model the new  $\widehat{U}$  couplings will be chosen at random (as opposed to the original  $U$  couplings which are determined by the deterministic algorithm (12) to give us the needed complex frustration). The random values of  $\widehat{U}$  will be selected, following [2], such that the new free energy will have the same high-temperature expansion as the original model. So, we will be in the typical situation described in [1, 2]. We will have a model where the couplings  $\widehat{U}$  will be distributed according to a probability distribution, determined from the need to find the same high- $T$  expansion as in the original frustrated

model. In this way the original model will be, by construction, a given (hopefully typical) realization of the coupling constants constructed according to this probability distribution.

Because of these remarks, and our constructive procedure, the deterministic model and the random one coincide in the high- $T$  phase. We hope to learn as much as possible about the low- $T$  phase, and that the two models are also very similar in this phase.

We will have to start by computing the high-temperature expansion for our model with complex frustration. Knowing that, we will use a reverse engineering procedure in order to find out the probability distribution of random couplings  $\widehat{U}$  that have the same high-temperature expansion. Finally we will use replica theory to compute the low-temperature behaviour of the random model. For the sake of simplicity, here we will present the computation done under the hypothesis of no replica-symmetry breaking. We will compare these analytic results to numerical simulations of the frustrated model.

We will consider a model containing quenched disorder that has the same form as the original model with complex deterministic frustration. In the random model the couplings  $\widehat{U}$  will be taken randomly among all matrices having the same spectral distribution of the deterministic model. More precisely for finite  $D$  we extract a set of  $2^D$  values of the eigenvalues  $\lambda$ , such that

$$2^{-D} \sum_{j=1,2^D} \lambda_j^n \simeq \int d\lambda \rho_\Delta(\lambda) \lambda^n \quad (25)$$

where  $\rho_\Delta$  is the spectral density of the Laplacian operator, and will be discussed in more detail in the next section. Finally, we set

$$\widehat{U}_{i,k} = \sum_{j=1,2^D} V_{i,j}^* \lambda_j V_{j,k} \quad (26)$$

where  $V$  is a random unitary matrix in a  $2^D$ -dimensional space.

#### 4. The high-temperature expansion

We have explained that we will construct the model based on the random couplings  $\widehat{U}$  by requiring that the high- $T$  expansion is the same as in the original model with complex frustration (and no disorder). Let us remark that both these models, the random one and the deterministic one, are *regular*, i.e. there are no couplings of  $O(1)$  when  $D \rightarrow \infty$ . In other words all the  $U$  couplings and the  $\widehat{U}$  ones, after being multiplied by the appropriate  $c(D)$  factor, go to zero in this limit. Under this condition the high-temperature expansion for the  $XY$  model (defined in (2) and (3)) is equal to the one of the spherical model (4) and (5). One can verify this statement by checking that in the two cases (i.e. for the spherical and for the  $XY$  model) the same diagrams survive in the  $D \rightarrow \infty$  limit. The regularity condition guarantees the absence of diverging couplings which could break the equivalence.

Thanks to this result we will be able to start by computing the high- $T$  expansion of the spherical model (4) and (5), in order to work out results valid for the  $XY$  model (which is the one we study numerically). That will make our task far easier.

We introduce the Laplacian operator  $\Delta$  defined as

$$(\Delta f)_j \equiv \sum_k U_{j,k} f_k. \quad (27)$$

We denote its spectral density by  $\rho_\Delta(\lambda)$ , and we express the trace of its  $n$ th moment as

$$2^{-D} \text{Tr}(\Delta^n) = \int d\lambda \rho_\Delta(\lambda) \lambda^n. \quad (28)$$



Here the trace is taken over a space of dimensionality  $2^D$ , and the normalizing factor  $2^{-D}$  is such that the spectral density of the identity operator  $\rho_1(\lambda)$  is  $\delta(\lambda - 1)$ .

We start by remarking that the internal energy density of the Gaussian model is given in terms of  $\rho_\Delta(\lambda)$  by

$$E_G = \int d\lambda \rho_\Delta(\lambda) \frac{\lambda}{1 - \beta\lambda}. \quad (29)$$

By using the expression of the Hamiltonian which includes the spherical constraint, equation (6), we see that analogously to (29) we find

$$E_S = \int d\lambda \rho_\Delta(\lambda) \frac{\lambda}{\mu(\beta) - \beta\lambda} \quad (30)$$

where  $\mu$  is a function of  $\beta$ . It is fixed by the condition

$$\int d\lambda \rho_\Delta(\lambda) \frac{1}{\mu(\beta) - \beta\lambda} = 1 \quad (31)$$

which tells that  $\langle \sum_i |\sigma_i|^2 \rangle = N$ , i.e. that the  $\sigma$  variables satisfy the spherical constraint (4).

Equations (30) and (31) can be written in a more compact form as

$$\mu(\beta) = R\left(\frac{\beta}{\mu(\beta)}\right) \quad (32)$$

$$E(\beta) = \frac{\mu - 1}{\beta} \quad (33)$$

where the function  $R$  is given by

$$R(z) = \int d\lambda \rho_\Delta(\lambda) \frac{1}{1 - z\lambda}. \quad (34)$$

One uses (32) to determine  $\mu$ , and inserting it in (33) one determines the internal energy density of the system.

The critical temperature  $\beta_c^{-1}$  is fixed by the condition that (32) does not admit a solution for  $\beta > \beta_c$ , i.e. is such that

$$z_c R(z_c) = \beta_c \quad (35)$$

where  $z_c$  is the inverse of the largest eigenvalue of  $\Delta$ .

In the limit  $D \rightarrow \infty$ , the function  $R(z)$  has been computed in [3]†. One finds that

$$G_n^{(q)} = \int d\lambda \rho_\Delta(\lambda) \lambda^n = \langle 0 | \mathcal{X}_q^n | 0 \rangle \quad (36)$$

where  $\mathcal{X}_q$  has been defined in (20).

It can be shown [3] that the function  $R(z)$  has a singularity of the form

$$R(z) = A(z_c^2 - z^2)^{1/2} \quad (37)$$

where

$$z_c = \frac{\sqrt{1-q}}{2}. \quad (38)$$

The critical behaviour does not depend on  $q$ .

The coefficients of the Taylor expansion of  $R(z)$  around  $z = 0$  can be easily evaluated on a computer. The time cost of the computation increases as the square of the order of the

† In the appendix to this paper we close a gap of the proof given in [3].

highest coefficient one wants to compute. The asymptotic behaviour of the coefficients for large  $z$  is controlled by the singularity closer to  $z = 0$ . If we define

$$R(z) = \sum_n R_n z^{2n} \tag{39}$$

we have that

$$\lim_{n \rightarrow \infty} R_n z_c^{2n} n^{3/2} \tag{40}$$

is finite and is given by

$$-\frac{Az_c}{2\pi^{1/2}}. \tag{41}$$

We want now to estimate the function  $R(z)$  starting from the knowledge of the first  $N$  coefficients of its expansion around  $z = 0$ .

Let us consider the function

$$r(z) \equiv \frac{2(1 - (1 - z^2)^{1/2})}{z^2} - 1 = \sum_n r_n z^{2n}. \tag{42}$$

Since

$$r_n \simeq \frac{n^{-3/2}}{\sqrt{\pi}} \tag{43}$$

equation (40) tells us that for large  $n$

$$R_n \simeq 2 A z_c^{-2n+1} r_n. \tag{44}$$

Let us say we have computed the coefficients  $R_n$  for  $n \leq N$ . We can use the two higher orders of the series to estimate  $A$  and  $z_c$ , which we will denote by  $A^{(N)}$  and  $z_c^{(N)}$ . They are determined by the relations

$$R_N = A^{(N)} r_N z_c^{(N)(-2N+1)} \quad R_{N-1} = A^{(N)} r_{N-1} z_c^{(N)(-2N-1)}$$

where  $r_N$  is the  $N$ th coefficient of the expansion of (42)

$$r_N = \frac{\Gamma(N + \frac{1}{2})}{\Gamma(N + 2)\Gamma(\frac{1}{2})}. \tag{45}$$

Now we assume that  $A^{(N)}$  and  $z_c^{(N)}$  are a good estimate for  $A$  and  $z_c$ , and that for  $n > N$  the coefficients  $R_n$  of the function  $R(z)$  are

$$R_n = A^{(N)} r_n z_c^{(N)(-2n+1)}. \tag{46}$$

We find that our assumption is equivalent to assuming that

$$R(z) = \sum_{n=0, N} (R_n - A^{(N)} z_c^{(N)1-2n}) z^{2n} + A^{(N)} z_c^{(N)} r \left( \frac{z}{z_c} \right). \tag{47}$$

The first  $N$  coefficients of the Taylor expansion of this function are exactly the  $R_n$ , since the two terms containing  $A^{(N)}$  cancel. The higher-order terms of the Taylor expansion of (47) are given by the terms (46).

We have tried in our computation two large values of  $N$ , i.e.  $N = 3 \times 10^3$  and  $N = 3 \times 10^4$ . We have computed the expansion of  $R(z)$  around  $z = 0$  up to order  $N$  in the two cases, and we have found a very similar estimate for  $R(z)$ . In the case where  $q = 0$  the function  $R(z)$  can be computed exactly [3], and it is given by  $r(\frac{z}{2})$ . In this case one can compute the exact expression for  $E(\beta)$ .

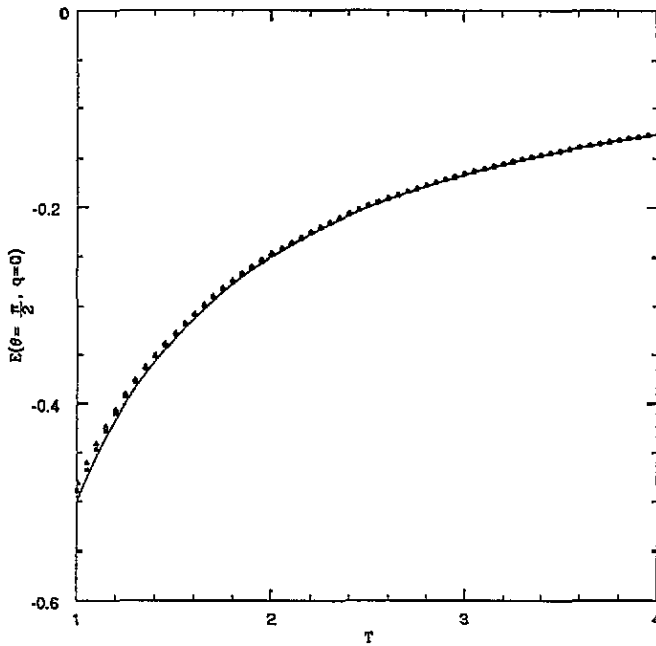


Figure 1. Energy of the  $q = 0$  model versus  $T$  in the high-temperature phase. The continuous line is from the resummation of the high- $T$  expansion, the points come from Monte Carlo simulations (for details see later in the text). In order to give a feeling for the finite-size effects we plot with full squares the data obtained on our larger lattice,  $D = 15$  and 32768 sites, and with open triangles data from a smaller lattice, with  $D = 12$ , i.e. 4096 sites.

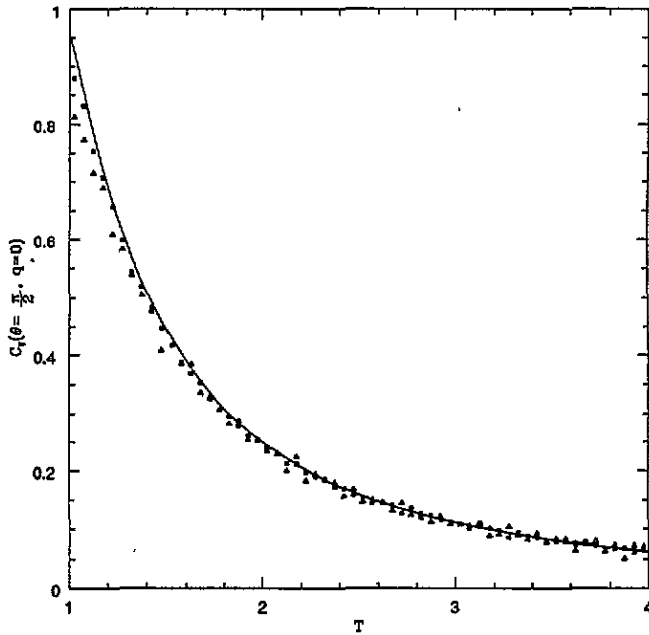
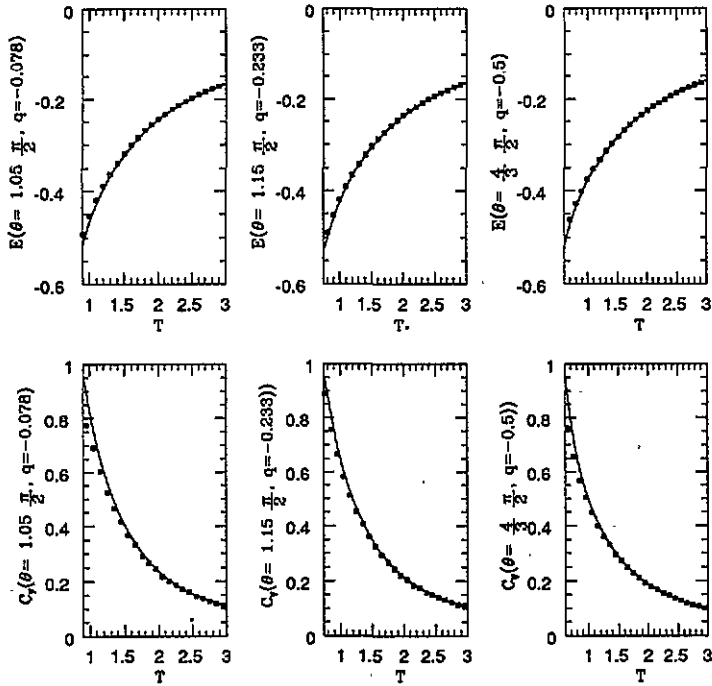


Figure 2. As in figure 1 but for the specific heat.



**Figure 3.** Energy and specific heat of the three models with  $q = -0.078$ ,  $-0.233$  and  $-0.5$  versus  $T$  in the high-temperature phase. The full curve comes from the resummation of the high- $T$  expansion, the points are from Monte Carlo simulations (for details see later in the text). Full squares are for the data obtained on our larger lattice,  $D = 15$  and 32768 sites.

We plot  $E(\beta)$  and the corresponding specific heat for the case  $q = 0$  in figures 1 and 2. For all values of  $q$  the specific heat at the transition point has the value of 1. The figures depict the high- $T$  phase, i.e. the region of  $T > T_c$  (which we know analytically). The agreement of the Monte Carlo data (which we will discuss in detail in the following) with the analytic solution looks quite good, even if on our larger lattice size we can still distinguish a clear finite-size effect.

In figure 3 we plot the energy and the specific heat for the three cases of  $q = -0.078$ ,  $-0.233$  and  $-0.5$ . The horizontal scale starts with the critical point. One can observe that the critical point shifts with  $q$ . In the specific heat finite-size effects are manifest close to  $T_c$ .

In figure 4 we plot the energy and the specific heat for the three analogous cases of positive  $q = 0.078$ ,  $0.233$  and  $0.5$ . Here the specific heat has a very sharp variation near the critical temperature. The variation becomes more and more abrupt for increasing values of  $q$ . The situation is dramatic at  $q = 0.5$ . Our analytic result does not succeed in reproducing the very sharp peak of the specific heat. Here we would have needed a very high accuracy in order to approximate the correct result. In this case in the high- $T$  side of the transition the points obtained by numerical simulations show, close to the critical point, very strong finite-size effects. It is remarkable how non-symmetric around  $q = 0$  the situation is. For  $q$  negative, i.e. in the direction of the fully-frustrated model, the system is changing quite smoothly. In contrast, for positive  $q$ , i.e. when approaching the ferromagnetic limit, the system changes very drastically. Indeed figure 4 shows that the change from  $q = 0.233$  to  $q = 0.5$  is very dramatic.

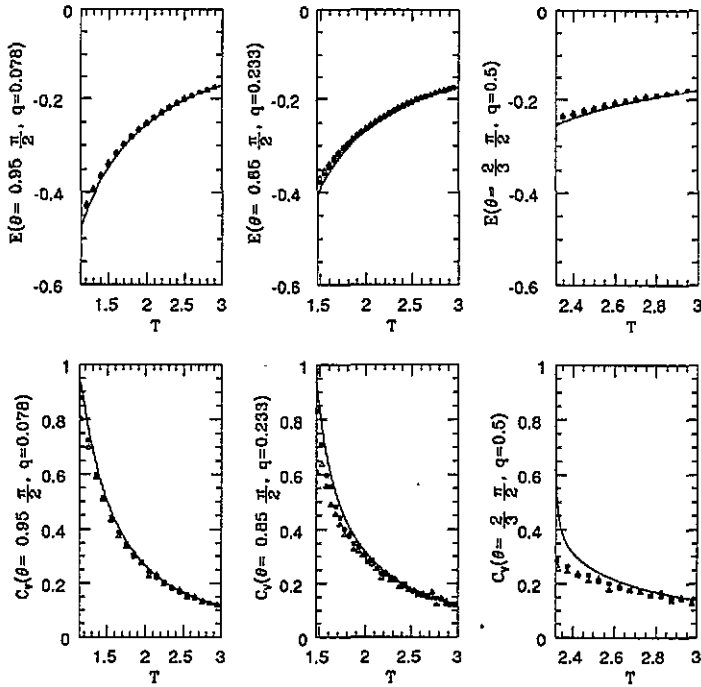


Figure 4. As in figure 3, but for  $q = 0.078, 0.233$  and  $0.5$ . Here we also add open triangles for a smaller lattice size, with the same notation as figure 1.

We can now summarize. Apart from the presence of such strong finite-size effects for high positive  $q$  the high-temperature analysis shows a very good agreement with the Monte Carlo data, which we will discuss in more detail in the following.

The spherical approximation is also correct in the high-temperature phase also for the model with quenched disorder. In fact, since the coupling matrices of the disordered model and of the deterministic one are isospectral the two models coincide in the spherical approximation and consequently in the high-temperature phase.

A last delicate point we want to discuss here is about the  $D \rightarrow \infty$  limit. The reader may wonder about the interchange of the limit  $D \rightarrow \infty$  with the limit  $\beta \rightarrow \beta_c$ . Is that safe? Could our theorems which allow us to solve the high-temperature phase of the model with complex frustration by using the  $q$ -deformed harmonic oscillator be spoiled by such an interchange? In order to be sure that nothing horrible happens (and also as an independent check of our numerical simulations) we have computed the function  $R_D(z)$  for a generic value of the dimension  $D$  up to the order  $z^{18}$ . This can be done by considering all different (apart from permutations) closed paths of up to 18 elements, and by computing their area and multiplicity. Since the total number of diagrams is 6 859 315 116 this computation can hardly be done by hand by simple enumeration. We preferred to let a computer accomplish the task for us.

We define the Taylor series for the finite-dimensional function  $R_D(z)$  as

$$R_D(z) = \sum_{k=0, \infty} R_D^k z^{2k}. \tag{48}$$

We also define

$$q_n \equiv \cos(n\theta) \tag{49}$$

where, obviously,  $q_1 = q$ . Here we give the full expression for the first five coefficients we have computed:

$$\begin{aligned}
 R_D^0 &= 1 & R_D^1 &= 1 \\
 R_D^2 &= \frac{(D-1)}{D}(2+q_1) + \frac{1}{D} \\
 R_D^3 &= \frac{(D-2)(D-1)}{D^2}(5+6q_1+3q_1^2+q_1^3) + \frac{(D-1)}{D^2}(9+6q_1) + \frac{1}{D^2} \\
 R_D^4 &= \frac{(D-3)(D-2)(D-1)}{D^3}(14+28q_1+28q_1^2+20q_1^3+10q_1^4+4q_1^5+q_1^6) \\
 &\quad + \frac{(D-2)(D-1)}{D^3}(56+86q_1+52q_1^2+16q_1^3) \\
 &\quad + \frac{(D-1)}{D^3}(34+28q_1+q_2) + \frac{1}{D^3}.
 \end{aligned} \tag{50}$$

Let us also define the leading contribution to  $R_D^k$  as the terms of order one which multiply the different powers of  $q_1$ , and the first one over  $D$  corrections analogously, i.e.

$$R_D^k \equiv \sum_{\alpha=0} \mathcal{R}^{k,\alpha} q_1^\alpha \left[ 1 - \frac{k(k-1)}{2D} \right] + \sum_{\alpha=0} \frac{\mathcal{S}^{k,\alpha}}{D} q_1^\alpha + O\left(\frac{1}{D^2}\right) \tag{51}$$

since the leading and the subleading terms in  $D$  contains only powers of  $q_1$  and not of the other  $q_n$ . In tables 1–9 we give all the  $\mathcal{R}^{k,\alpha}$  and the  $\mathcal{S}^{k,\alpha}$  we have computed. We hope that this information maybe useful for a possible analytic computation of the  $\frac{1}{D}$  corrections.

Table 1. The coefficients  $\mathcal{R}^{k,\alpha}$  for  $\alpha$  going from 0 to 6.

$k$	$\alpha$						
	0	1	2	3	4	5	6
0	1						
1	1						
2	2	1					
3	5	6	3	1			
4	14	28	28	20	10	4	1
5	42	120	180	195	165	117	70
6	132	495	990	1430	1650	1617	1386
7	429	2002	5005	9009	13013	16016	17381
8	1430	8008	24024	51688	89180	131040	169988
9	4862	31824	111384	278460	556920	946764	1419432

Table 2. As in table 1 but for  $\alpha$  going from 7 to 12.

$k$	$\alpha$					
	7	8	9	10	11	12
5	35	15	5	1		
6	1056	726	451	252	126	56
7	16991	15197	12558	9646	6916	4641
8	199264	214578	214760	201460	178248	149464
9	1922904	2394450	2775080	3021444	3112632	3051024

Table 3. As in table 1 but for  $\alpha$  going from 13 to 18.

$k$	$\alpha$					
	13	14	15	16	17	18
6	21	6	1			
7	2912	1703	924	462	210	84
8	119 168	90 540	65 640	45 438	30 024	18 908
9	2 858 040	2 567 340	2 217 480	1 845 486	1 482 264	1 150 220

Table 4. As in table 1 but for  $\alpha$  going from 19 to 25.

$k$	$\alpha$						
	19	20	21	22	23	24	25
7	28	7	1				
8	11 320	6 420	3 432	1 716	792	330	120
9	862 920	626 076	439 263	297 891	195 075	123 165	74 817

Table 5. As in table 1 but for  $\alpha$  going from 26 to 36.

$k$	$\alpha$										
	26	27	28	29	30	31	32	33	34	35	36
8	36	8	1								
9	43 605	24 293	12 870	6 435	3 003	1 287	495	165	45	9	1

Table 6. The coefficients  $S^{k,\alpha}$  for  $\alpha$  going from 2 to 6.

$k$	$\alpha$						
	0	1	2	3	4	5	6
2	1						
3	9	6					
4	56	86	52	16			
5	300	740	880	690	370	140	30
6	1 485	5 082	8 904	10 818	10 020	7 494	4 611
7	7 007	30 758	70 707	114 471	145 264	153 377	139 286
8	32 032	171 808	486 920	976 520	1 548 952	2 064 048	2 395 464
9	143 208	908 208	3 052 656	7 265 664	13 712 319	21 806 163	30 323 493

Table 7. As in table 6 but for  $\alpha$  going from 7 to 12.

$k$	$\alpha$					
	7	8	9	10	11	12
6	2 310	927	276	48		
7	110 691	77 882	48 727	26 964	13 020	5 397
8	2 476 448	2 316 576	1 981 972	1 560 904	1 135 608	764 856
9	37 776 564	42 883 740	44 909 478	43 774 344	39 972 618	34 364 322

**Table 8.** As in table 6 but for  $\alpha$  going from 13 to 18.

$k$	$\alpha$					
	13	14	15	16	17	18
7	1 848	476	70			
8	476 704	273 784	143 804	68 424	29 116	10 800
9	27 912 096	21 466 764	15 650 046	10 819 422	7 090 146	4 396 734

**Table 9.** As in table 6 but for  $\alpha$  going from 19 to 28.

$k$	$\alpha$									
	19	20	21	22	23	24	25	26	27	28
8	3 312	752	96							
9	2 571 534	1 411 929	723 609	343 611	149 490	58 410	19 800	5 490	1 116	126

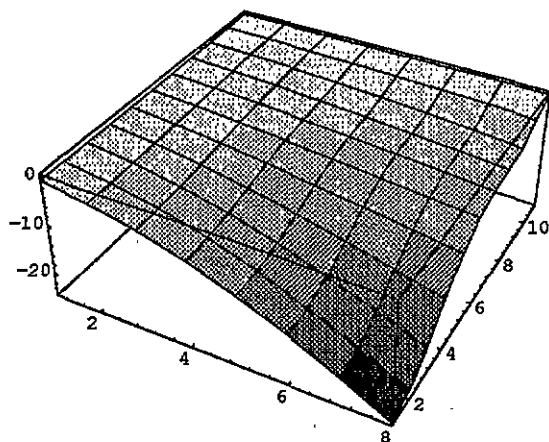


**Figure 5.**  $\Omega^k$  versus  $k$  going from 2 to 9. The axis labelled with 2, 4, 6 and 8, on the left, is  $k - 1$ . The axis with labels going up to 10, on the right, is the  $\theta$  axis.  $\theta$  goes from 0 to  $\pi$ .  $\theta = 0$  coincides with the tick 1,  $\theta = \frac{\pi}{2}$  with the tick 6 and  $\theta = \pi$  with the tick 11.  $q = 1$  on the left limit of the axis (ferromagnet),  $q = 0$  (spin glass) in the centre and  $q = -1$  (fully-frustrated model) on the right edge of the axis. The vertical axis is for  $\Omega^k$ . Decreasing values of  $\Omega^k$  are drawn with heavier shading.

For analysing the large  $D$  behaviour of our series is useful to define the expansion

$$R(z) = \sum_k z^{2k} \sum_\delta \bar{R}_\delta^k D^{-\delta} \quad (52)$$

where the  $\delta = 0$  contribution is the leading term of the  $D^{-1}$  expansion. We define the quantity

$$\Omega^k(\theta) \equiv \frac{\bar{R}_0^k}{\bar{R}_1^k} \quad (53)$$

which is related to the convergence radius of the  $k$ th term in  $D^{-1}$ . It is indeed easy to see that in the large  $D$  and large- $k$  limit

$$\Omega^k(\theta) \simeq k(C(D) - C(\infty)) \quad (54)$$

where  $C(\infty)$  is the radius of convergence of the perturbative series in  $D = \infty$ , and  $C(D)$  is the radius of convergence of the series in a finite number of dimensions  $D$ .

We plot the  $\Omega$  surface as a function of  $k$  and  $\theta$  in figure 5. It is interesting to note that moving away from  $\theta = \frac{\pi}{2}$  in the direction of the fully-frustrated model, i.e. increasing  $\theta$ ,  $\Omega$



changes quite smoothly. In contrast when  $\theta$  becomes smaller than  $\theta = \frac{\pi}{2}$  the change is far more abrupt. This is coherent with what we find from figure 3 where for negative values of  $q$  the system does not change much, and figure 4 where  $q > 0$  the system undergoes a strong quantitative change around  $q = \frac{1}{2}$ . This point is where in figure 5 we can find a maximal change of  $\Omega$  as a function of  $q$ .

We have also checked that the results are in reasonable agreement with the ansatz

$$\frac{R_D^k}{R_D^{k-1}} = a + \frac{b(\frac{k}{D})}{D} \tag{55}$$

where the function  $b(w)$  does not seem to have a fast divergence for large values of  $w$ . Apparently the limit  $D \rightarrow \infty$  is smooth.

### 5. The low-temperature region

In the previous section we have discussed the high- $T$  region of the deterministic model with complex frustration. We have shown that the Monte Carlo data reproduce well (but for the case of high, positive  $q$ , where finite-size effects are dramatic) the series obtained by computing the Green functions of the  $q$ -deformed harmonic oscillator. Together with the results of [3] and the appendix of this paper that makes the status of the high- $T$  phase clear. We also know that in the high- $T$  phase the model with quenched disorder coincides by construction with the deterministic model, but we will see that better in the following.

In order to get information about the low- $T$  phase we have to use the random model, which we have defined in (25) and (26). We will use replica theory to solve it both in the high- $T$  phase (where we will again find the same high- $T$  series) and in the low- $T$  phase. We will try to understand how much the replica formulation of the system is connected to the Monte Carlo data we will get directly from the deterministic model with complex frustration.

Let us solve the random model by using the techniques introduced in [1, 2]. The computation follows quite closely the one of [1, 2], and here we will give only the main details. One introduces  $n$  replicas, where  $n$  has to be sent to zero at the end of the computation. The  $n$ -dependent free energy is given by

$$f^{(n)}(\beta) \equiv -\lim_{N \rightarrow \infty} \frac{1}{\beta N} \frac{\bar{Z}_U^n - 1}{n} \tag{56}$$

where the bar denotes the average over the random couplings and the replicated partition function  $Z_U^n$  depends over the noise and can be written as

$$Z_U^n \equiv \int [d\sigma] e^{-\beta \sum_{a=1}^n H_U^a} \tag{57}$$

The integration over the unitary group can be done explicitly. After some algebra one finds that one has to evaluate the stationary points of the following free energy:

$$A[Q, \Lambda] = -\text{Tr} G(\beta Q) + \text{Tr}(\Lambda Q) - F(\Lambda) \tag{58}$$

where  $Q$  and  $\Lambda$  are  $n \times n$  matrices, the function  $G$  is related to the one defined in (33) by

$$\frac{dG}{dz} \equiv E(z) \tag{59}$$

and

$$F(\Lambda) \equiv \ln \int d[\sigma] \exp\left(\sum_{a,b} \Lambda_{a,b} \sigma^a \sigma^b\right) \tag{60}$$

In the high-temperature phase the off-diagonal terms of the two matrices  $Q$  and  $\Lambda$  are zero. If we set

$$Q_{a,b} = \delta_{a,b} q \quad \Lambda_{a,b} = \delta_{a,b} \lambda \quad (61)$$

we find that the stationary equations imply that

$$q = 1 \quad \text{and} \quad \lambda = E(\beta). \quad (62)$$

Finally we find that in the high-temperature phase

$$\frac{\partial F}{\partial \beta} = E(\beta) \quad (63)$$

where  $E(\beta)$  is the function defined in (59). In this way we have again derived the equivalence of the model with quenched disorder and the deterministic model with complex frustration in the high-temperature phase.

In the low-temperature region the off-diagonal terms of the two matrices are non-zero. If we assume that replica symmetry is unbroken, we have that the off-diagonal terms† are given by

$$Q_{a,b} = q \quad \Lambda_{a,b} = \lambda. \quad (64)$$

In this way we find that we have to minimize the free energy

$$G(\beta(1-q)) + \beta q E(\beta(1-q)) - \lambda q + f(\lambda) \quad (65)$$

where the function  $f$  is given by

$$\ln \left( \int dh \exp(-h^2/2) \right) \ln \left( \int d\sigma_r d\sigma_i \delta(\sigma_r^2 + \sigma_i^2 - 1) \exp(-\lambda^{1/2} h \sigma_r) \right). \quad (66)$$

The energy turns out to be

$$E(\beta) = G'(\beta(1-q)) - \beta q(1-q)G''(\beta(1-q)). \quad (67)$$

By deriving this expression and evaluating it for  $\beta = \beta_c$  we find that

$$C_V(\beta_c^+) = C_V(\beta_c^-) = 1. \quad (68)$$

The critical temperature can also be determined through the relation

$$\beta_c^2 G''(\beta_c) = 1. \quad (69)$$

One also finds that at zero temperature

$$C_V(\infty) = \frac{1}{2} \quad (70)$$

in agreement with the equipartition theorem.

The equations which determine the minimum of such free energy can be solved numerically.

We will show and discuss their solution in the next section, for different  $q$  values, together with the Monte Carlo results in the low- $T$  phase.

We expect the unbroken replica solution to give rather accurate values for the free energy. In the SK model the error over the correct, replica-broken result is smaller than 3%, and it is likely to be even smaller in the present case. It is interesting to note that the replica-symmetric solution normally gives a lower bound to the true free energy and to the true internal energy of the system. Our numerical simulations show that when we compare numerical simulations of the deterministic model to the replica-symmetric solution of the disordered model in the cold phase this is not always the case in our system, pointing to a non-complete coincidence of the two models.

† We set  $Q_{a,a}=1$ . The value we chose for  $\Lambda_{a,a}$  is irrelevant, and does not change the results.

## 6. Computer simulations

Here we will describe our numerical simulations of the model with complex frustration and no quenched disorder (but for the small one needed for constructing the antisymmetric tensor  $\mathcal{S}$ ), defined with the couplings of (12), and compare them with the analytic solution of the model with quenched disorder that we have discussed in the previous section. Here we will mainly focus on the low- $T$  phase.

We have simulated systems with  $D$  going from 3 to 15 or 16, i.e. containing from 8 to 32 768 or 65 536 sites. We have been starting from all fields set to 1 at high  $T$ , and decreased the temperature in small steps. A typical pattern has been starting from  $T = 4.05$ , and decreasing it down with 80 steps of  $\Delta T = 0.05$  (but for some runs we only used 40 steps and a lower starting point). At each next  $T$  we have been continuing from the last configuration obtained at  $T + \Delta T$ . At each  $T$  value we have used 500 full sweeps of the system to obtain an acceptance value of the Monte Carlo procedure of 50% (by tuning the angular increment we would propose for updating the field phase in a given site). After that we have used 1250 full sweeps to thermalize the system, and 5000 full sweeps to measure the internal energy. We have run some longer simulations to check that we have indeed reached thermal equilibrium, and it seems to be the case. We believe that the statistical error on our data points is always smaller than the symbols we use to plot them. In the final plots we have always only used the data from a single realization of the antisymmetric tensor  $\mathcal{S}$  (even if we have checked the size of typical fluctuations by simulating more than one  $\mathcal{S}$  set, and the induced uncertainty turned out to be not very large, but detectable).

As a first check we have verified we could reproduce the results obtained in [4] for the fully-frustrated model.

A second preliminary question was concerning the equality of the traces of the  $n$ th powers of the coupling matrix and the expectation values of the operators which appear in the formalism of the  $q$ -deformed harmonic oscillator. This is a point which has been proved in [3] and in this paper, and verifying it was meant to constitute both a check of our codes and of our theorems. So given the couplings we have selected, according to (12) and to a random choice of the  $\mathcal{S}$  (over which in this case we have averaged) we have verified that

$$2^{-D} \text{Tr}(\Delta_q^n) = \langle 0 | \mathcal{X}_q^n | 0 \rangle. \quad (71)$$

In this case we have kept the statistical error (given in this case by the distribution of the  $\mathcal{S}$ , and not by a Monte Carlo: there is no Monte Carlo here!) under careful control. All momenta up to  $n = 8$  coincide with the  $q$ -deformed result with a precision better than  $10^{-3}$ . Our best fits give the right answer, with a  $\chi^2$  of the order of one per degree of freedom. So, this check has been positive, and it is an important check of the equivalence of the model with complex frustration and the random model in the high- $T$  phase.

We now come to the main point of our investigation, i.e. the low- $T$  phase. Here we will compare the analytic solution† of the random model (25) with the numerical simulation of the deterministic model. We will see that the data are indicative of a strong similarity, but not of a complete equivalence of the two models.

In figure 6 we plot the energy of the  $q = 0$  model versus  $T$ , in both phases (the critical point is at  $T_c = 1$ ). Here and in the following figures the point where the broken curve becomes continuous is the critical point. We plot the analytic result from the high- $T$  expansion with a broken curve, while the result obtained by minimizing (65) is plotted with a full curve, for  $T < T_c$ . Here we include the data from all our simulations. The starred

† We will use the replica-symmetric solution, which we believe is not too wrong, as we have explained in the previous section.

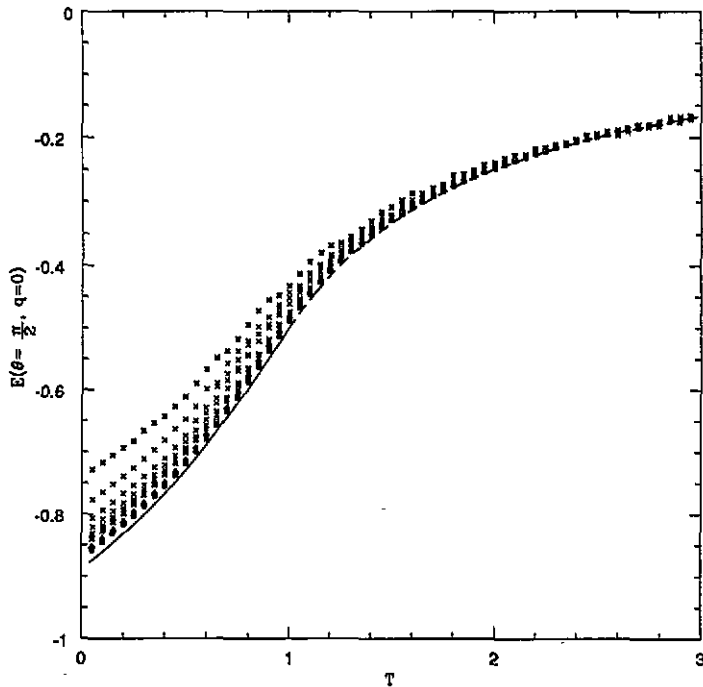


Figure 6. Energy of the  $q = 0$  model versus  $T$ . Here we are looking at both phases (the critical point is at  $T_c = 1$ ). See the text for the explanation of the different symbols. The point where the broken curve becomes continuous is the critical point here and in the following figures.

dots, lying at the top, are from  $D = 3$ . Crosses are for intermediate values of  $D$  (lower points for higher  $D$  values). For the four higher values of  $D$  (in this case  $D = 13, 14, 15$  and  $16$ ) we change symbol again, and use open triangles, open squares, full triangles and full squares, respectively.

The agreement of Monte Carlo data for the deterministic model and replica-symmetric solution of the random model is also quite good in the broken phase, for  $T < T_c$ . We expect that the solution with broken replica symmetry will have an energy slightly higher than the unbroken one (as we have already said, in the general case the replica-symmetric energy is a lower bound to the true energy of the physical system). The very small residual finite-size effect, and this small energy drift to the breaking of replica symmetry should explain the small discrepancy between the numerical data and the analytic curve. So in the case of the  $q = 0$  model things seem to go smoothly.

When moving on the side of negative  $q$  values things do not change much, and if there is a discrepancy it is very small. This is completely consistent with the discussion of the behaviour of the coefficients of the high- $T$  expansion of the previous section.

Figures 7 and 8 allow, by presenting the results together, a direct comparison of the effect of the  $q$  perturbations of opposite sign. In figure 7(a) the results for  $q = -0.233$  are shown (where the angle is already different by 15% from  $\theta = \frac{\pi}{2}$ ). The agreement of our data with the analytic solution is still quite good. Figures 6 and 7(a) are on the same scale (as will be all the following energy plots). This allows the reader to appreciate that the two energy plots are indeed quite different. To show even better that things are basically working in this regime of negative  $q$  values we plot in figure 8(a) the specific heat for

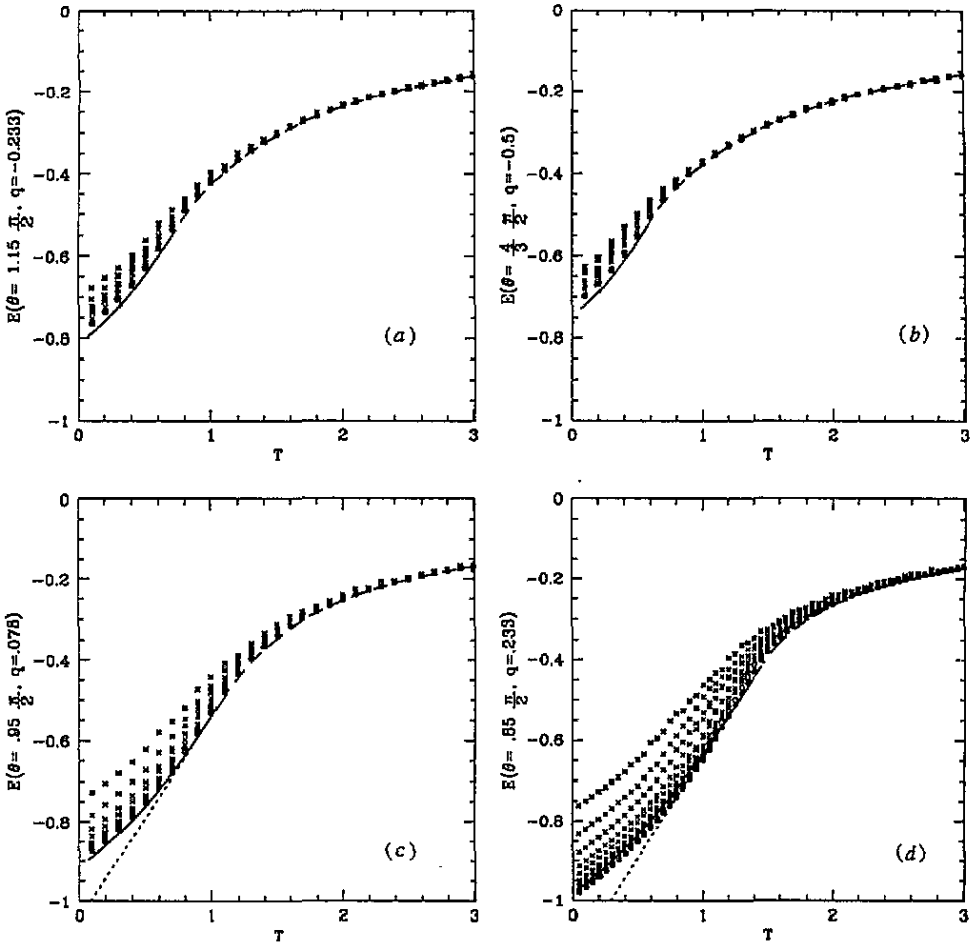


Figure 7. As in figure 6, but for (a)  $q = -0.233$ ; (b)  $q = -0.5$ ; (c)  $q = +0.078$ ; (d)  $q = +0.233$ .

$q = -0.233$ . The small gap in the analytic curve close to the maximum is because we stopped our numerical evaluation of the high- $T$  series early. Here we cannot detect any clear discrepancy.

We show in figures 7(b) and 8(b) that even at very high negative values of  $q$  (i.e. at least down to  $q = -0.5$ ) our replica solution of the model with quenched disorder gives a very accurate description of the behaviour of the deterministic model with complex frustration in the low- $T$  phase. Even the specific heat very close to the critical point is reconstructed with good accuracy.

The situation is different on the side of  $\theta < \frac{\pi}{2}$ , i.e. for positive values of  $q$ . At low positive  $q$  there are again no dramatic problems, and if the two models differ they differ only in a very minor way. In figure 7(c) we add a broken straight line, from  $T_c$  down to  $T = 0$ , to give the result one would obtain for the spherical model [13], where the energy becomes linear in  $T$  below the critical point. In figure 8(c) we again plot the specific heat. If there is a discrepancy it is small, even if we already want to notice the small bump just under  $T_c$ , which makes the Monte Carlo data slightly different from the disordered model

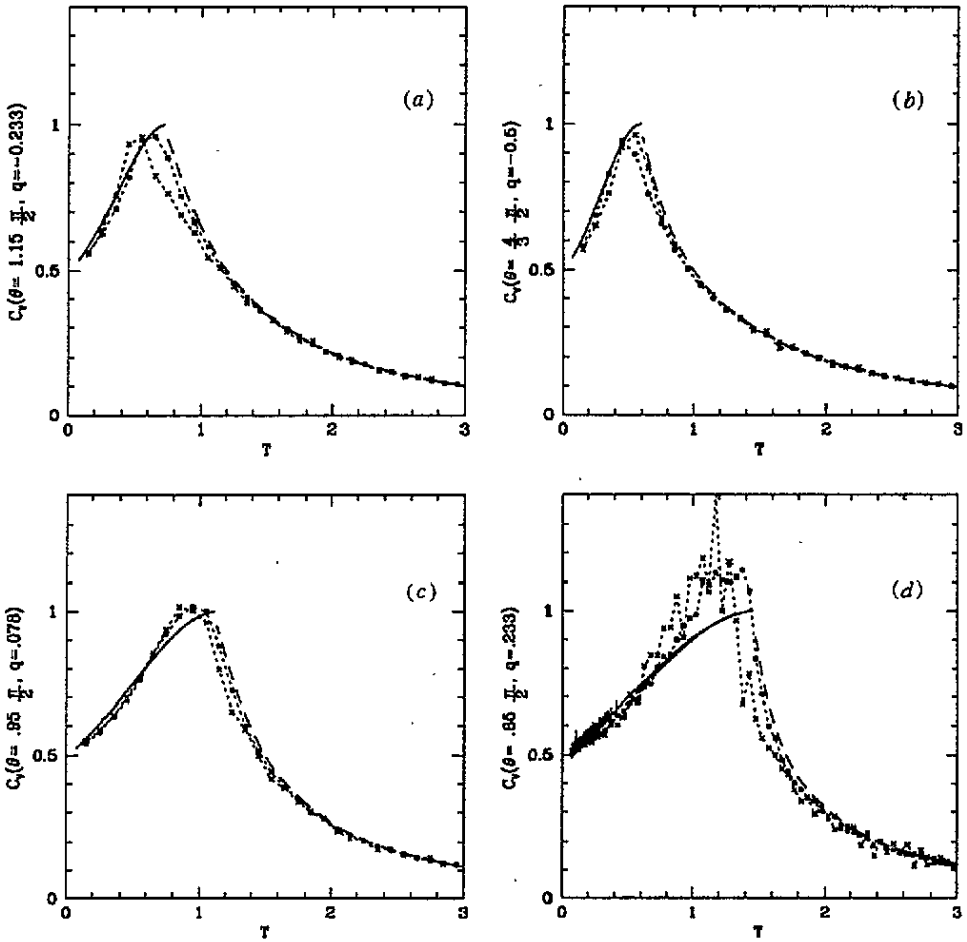


Figure 8. As in figure 7, but the specific heat  $C_V$ , with the same four  $q$  values. For the sake of clarity here we only use crosses for  $D = 12$  data and full squares for  $D = 16$ , and we join the data points with dotted lines.

result. This effect was not there for negative  $q$  values, and it is not clear here if it is due to a true difference or if it is connected to a finite-size effect.

The situation becomes more clear (in a negative sense) when we increase  $q$  slightly. In figures 7(d) and 8(d) we give the results for  $q = 0.233$ , and here there is a clear discrepancy, which is difficult to justify by means of finite-size effects. Indeed here the energy of the Monte Carlo simulations at low- $T$  is for  $D = 16$  already lower than the analytic result one gets for the spherical random model in the infinite-volume limit. Since the energy is decreasing with  $D$ , and we expect the energy of the spherical model to be a lower bound at all  $T$  to our  $XY$  case, this seems to show that in this case the two models do indeed differ, even if only by a small amount. In order to explain this effect one would have to assume that the sign of the corrections changes with the dimensionality, and that the energy will go up again for  $D$  large enough. This is not impossible, but not so plausible, and we have no numerical indications of such an effect to be taking place. The specific heat picture (figure 8(d)) is even more self-explanatory than the energy, since it is quite difficult

to believe that the big bump of the Monte Carlo data will be reabsorbed in the  $D \rightarrow \infty$  limit.

In conclusion, it seems that for  $q < 0$  and even for small  $q$  positive values the replica theory describes the deterministic model with very high accuracy. In contrast, for  $q > 0$  and not so small there is a clear, even if quite small discrepancy between the two models.

## Appendix

In this short appendix we will fill a gap in the proof of (36). We only sketch the main steps of the proof, which is absolutely inelegant. It is quite likely that a more elegant proof, e.g. based on the braid group, does exist, but we have not found it.

In [3] it was proved that

$$G_k^{(q)} \equiv \int d\lambda \rho_\Delta(\lambda) \lambda^n = \sum_{n=0, \infty} \mathcal{N}(k, n) q^n \quad (\text{A1})$$

where  $\mathcal{N}(k, n)$  is the number of ways in which one can piecewise connect  $k$  points on a circle, with  $n$  intersections.

In order to compute  $\mathcal{N}(k, n)$  it may be convenient to consider the quantity  $\mathcal{N}(k, n, m)$ , i.e. the number of ways in which  $k + 1$  points on the circle may be connected in such a way that a line starts from each of the first  $k$  points and  $m$  lines arrive in the last  $(k + 1)$ th point, the total number of intersections being  $n$ . It is evident that

$$\mathcal{N}(k, n) = \mathcal{N}(k, n, 0). \quad (\text{A2})$$

A simple pictorial argument can be used to prove that

$$\mathcal{N}(k + 1, n, m) = \mathcal{N}(k, n, m - 1) + \sum_{j=0, m} \mathcal{N}(k, n - j, m + 1). \quad (\text{A3})$$

We can now check that this relation is satisfied if we set

$$\sum_{n=0, \infty} \mathcal{N}(k, n, m) q^n \equiv G_k^{(q)}(m) = \langle m | Y^k | 0 \rangle \quad (\text{A4})$$

where the  $|n\rangle$  (for  $n = 0, \infty$ ) form a basis in a Hilbert space,

$$Y \equiv A + A^\dagger \quad (\text{A5})$$

and

$$\begin{aligned} A|n\rangle &= |n - 1\rangle \quad \text{for } n \neq 0 \\ A|0\rangle &= 0 \\ A^\dagger|n\rangle &= \frac{1 - q^{n+1}}{1 - q} |n + 1\rangle. \end{aligned} \quad (\text{A6})$$

The operator  $X$  in (36) and  $Y$  are related by the simple transformation  $X = MYM^{-1}$ , where the operator  $M$  is diagonal in the basis we have used. Finally we find that

$$G_k^{(q)}(0) = \langle m | Y^k | 0 \rangle = \langle m | X^k | 0 \rangle \quad (\text{A7})$$

which is the result announced in [3].

**References**

- [1] Marinari E, Parisi G and Ritort F 1994 *J. Phys. A: Math. Gen.* **27** 7615
- [2] Marinari E, Parisi G and Ritort F 1994 *J. Phys. A: Math. Gen.* **27** 7647
- [3] Parisi G 1994 *J. Phys. A: Math. Gen.* **27** 7555
- [4] Marinari E, Parisi G and Ritort F 1995 *J. Phys. A: Math. Gen.* **28** 327
- [5] Parisi G 1992 *Field Theory, Disorder and Simulations* (Singapore: World Scientific)
- [6] Huse D A and Seung H S 1990 *Phys. Rev. B* **42** 1059
- [7] Reger J D, Tokuyasu T A, Young A P and Fisher M P A 1991 *Phys. Rev. B* **44** 7147
- [8] Gingras M J P 1992 *Phys. Rev. B* **45** 7547
- [9] Parisi G 1988 *Statistical Field Theory* (Redwood City, CA: Addison Wesley)
- [10] Kirkpatrick S and Sherrington D 1978 *Phys. Rev. B* **17** 4384
- [11] Brezin E, Itzykson C, Parisi G and Zuber J B 1978 *Commun. Math. Phys.* **59** 35
- [12] Bouchaud J P and Mezard M 1994 *J. Physique I* **4** 1109
- [13] Kosterlitz J M, Thouless D J and Jones R C 1976 *Phys. Rev. Lett.* **36** 1217